Ballistic delivery of compounds to inner layers of the cornea is limited by tough mechanical properties of stromal tissue

Benjamin Laccetti, Julia Kornfield

PII: S1751-6161(20)30785-2

DOI: https://doi.org/10.1016/j.jmbbm.2020.104246

Reference: JMBBM 104246

To appear in: *Journal of the Mechanical Behavior of Biomedical Materials*

Received Date: 10 July 2020

Revised Date: 19 November 2020

Accepted Date: 29 November 2020

Please cite this article as: Laccetti, B., Kornfield, J., Ballistic delivery of compounds to inner layers of the cornea is limited by tough mechanical properties of stromal tissue, *Journal of the Mechanical Behavior of Biomedical Materials* (2021), doi: https://doi.org/10.1016/j.jmbbm.2020.104246.

Author Statement

Manuscript Title: *Ballistic Delivery of Compounds to Inner Layers of the Cornea is Limited by Tough Mechanical Properties of Stromal Tissue*

Benjamin Laccetti: Methodology, Software, Validation, Formal Analysis, Investigation, Data Curation, Writing (Original Draft), Visualization. **Julia Kornfield:** Conceptualization, Writing (Review and Editing), Supervision, Project Administration, Funding Acquisition.

Ballistic Delivery of Compounds to Inner Layers of the Cornea is Limited by Tough Mechanical Properties of Stromal Tissue

Benjamin Laccetti* and Julia Kornfield

Department of Chemical Engineering, California Institute of Technology, Pasadena, California 91125, USA

*Correspondence to author. blaccett@caltech.edu (B. Laccetti)

Abstract

The barrier characteristics of the cornea are interrogated using the impact of micro-particles into *ex vivo* porcine cornea. Using a commercial gene gun (BioRad; PDS1000), microparticles were accelerated and made to embed in target materials: either ballistic gelatin as a reference or corneal tissue. Statistical analysis of penetration of polydisperse spherical microparticles (5 to 22 μm dia.) with density of 2.5 g/cc, 4.2 g/cc, and 7.8 g/cc (soda-lime glass, barium-titanate glass and stainless steel; more limited examination of 1.1 g/cc polyethylene and 19.2 g/cc tungsten) spanned almost two decades in kinetic energy. Penetration profiles in ballistic gelatin show that the particle embedding depth is sensitive to particle size and density. In the cornea, penetration is a weak function of size and density, and the corneal stroma is an effective stopping medium for high velocity microparticles. Despite the high water content of corneal tissue (76 % w/w) compared to the stratum corneum of skin (40 % w/w), the resistance to penetration of the cornea is comparable to what is seen in previous research of penetration in skin tissue. Using low density polymer particles with a therapeutic agent payload, it is demonstrated that bulk material can be ballistically delivered to the central 1 cm^2 of the corneal epithelium in an even layer with high bioavailability of therapeutic compound.

Keywords:
cornea; drug-delivery; keratoconus; gelatin; penetration.

1. Introduction

Drug delivery to the cornea is limited by several mechanisms. Natural lacrimation and blinking remove hydrophilic drugs, and the corneal epithelium (a lipophilic tissue layer) has tight junctions between stratified epithelial cells that prevent many drugs from diffusing into the tissue (Ableson et al., 2009). Enhancing drug uptake into the cornea has the potential to improve treatments for diseases of the eye. For example, Novosorb, a cationic emulsion which binds to the mucin layer on the eye's anterior surface (made by PolyNovo), has had success in delivering latanoprost, a prostaglandin analog which lowers intraocular pressure for patients with glaucoma (Daull et al., 2017). The following work investigates high velocity microparticle bombardment as a means of embedding drugs in the cornea's epithelial barrier. An example that illustrates the range of particle size and corresponding number of particles to deliver a relevant dose of drug is delivery of cross-linking therapeutic to treat corneal ectasias. Corneal cross-linking surgery (CXL), a procedure in which photosensitizing cross-linking agents are used to reinforce the mechanical properties of the cornea (Gordon-Shaag et al., 2015), requires delivery of cross-linking agents (e.g. riboflavin and Eosin Y) to the stroma. Slow transport through the epithelium is usually overcome by removing the epithelium to access the stromal layer. Techniques to improve the flux of cross-linker are under development, like the use of iontophoresis and proteins that disrupt epithelial tight junctions, but in the US epithelium-off CXL remains the standard of care for keratoconus, despite a reduction in post-operative complications (Cifariello et al., 2018; Jia et al., 2018; Bidwell et al., 2014). If particles with a large volume fraction of drug were used, a sufficient dose might be provided biolistically to deliver 6,000 particles of 30 μm diameter distributed across 1 cm^2 of corneal tissue, potentially in the blink of an eye (Huynh 2011).

Our work builds on established "biolistic" techniques to introduce DNA through the cell membrane of cells at the exposed surface of a tissue using nucleic-acid-coated metal microparticles delivered to tissue at high velocity. Originally intended to transfect maize cells through their tough cell walls, this technology is now used to deliver genes to both plants and animal tissues, including corneal tissue (Lu et al., 2003; Tanelian et al., 1997). For example, to improve the acceptance rates of corneal transplants, biolistic

gene delivery has been used *in vivo* to enable epithelial cells to produce cytotoxic T-lymphocyte-associated protein 4 (Zhang et al., 2002; Merediz et al., 2000). In the context of skin and mucosal tissue, biolistic methods have been extended to deliver drugs, rather than genes, using larger particles (20 to 40 μm dia.) (Kendall et al., 2000; Mitchell et al., 2003). However, therapeutic particle delivery to the corneal stroma, to the best of our knowledge, has not been investigated.

Penetration of foreign bodies into the cornea have examined larger particles (~1 mm and larger) often related to wood and metal working or exposure to explosions in mines or warzones. After blast injuries, particularly improvised explosive device (IED) and mine-blast injuries, there are often multiple deep stromal foreign bodies in exposed corneal tissue (Camodeca et al., 2020; Gumus et al., 2007; Scott, 2011). To enable biolistic drug delivery, a detailed study is required to determine "kinetic impact parameters" (i.e. particle density, size, and impact velocity) that can successfully deliver therapeutics to the cornea.

Following Kendall and coworkers, we use polydisperse spherical particles (exploring, a range of particle sizes in parallel) and use a series of different with densities from that typical of biological tissues (i.e. 1 g/cm^3) to almost 20-times greater density. This allows us to investigate a wide range of kinetic energies and to efficiently establish relationships between size and embedding depth. This work compares ballistic gelatin and corneal tissue, revealing a dichotomy between penetration in a homogenous, isotropic material and a tissue that has distinct layers (i.e., pronounced heterogeneity in the direction normal to particle penetration). Gelatin conforms with theory, showing proportionality between particle size and penetration depth. In contrast, particles pile up at the tough stromal interface of corneal tissue, even when they have sufficient kinetic energy to penetrate deeply into ballistic gelatin.

2. Materials and Methods

2.1. Preparation of Ballistic Gelatin and Corneal Tissue Samples

Ballistic gelatin is a material with consistent mechanical properties used in ballistics research. Gels were prepared using the standard protocol (Jussila et al., 2004) at three concentrations of 2.5, 5.0 and 10.0% w/w. Gelatin samples were allowed to solidify for 24 hours at room temperature and then for 24 hours at 4°C.

Porcine eyes were acquired and used within 24 hours of animal sacrifice (Sierra Medical Products). They were kept in antibiotic medium until they were trimmed of surrounding tissue and kept moist with phosphate buffered saline (PBS) prior to microparticle treatment.

2.2. Gene Gun and Ballistic Microparticles Used

A BioRad PDS-1000 gene gun (catalog #: 1652257) was used to deliver high-velocity microparticles following protocols described in Sanford et al., 2003. In brief, a payload of microparticles of interest is placed on a Kapton disc (macrocarrier) that is mounted below the gas acceleration tube of the device. A rupture disc that bursts at a prescribed pressure (1350 PSI, 92bar) is mounted in the gas acceleration tube. The sample chamber is then pumped down to approximately 23mm Hg to maximize payload acceleration (the sample is exposed to vacuum for approximately 30s). The gas acceleration tube is pressurized with a desired carrier gas (helium); when the rupture pressure is reached, the gas expands, accelerating the macrocarrier in a reproducible manner. Particles release from the macrocarrier when it is abruptly stopped by a wire mesh that allows microparticles to pass (1 cm flight length).

Five polydisperse microparticle materials were chosen to span the desired density range. In Table 1, the range of tested microparticle composition, size, and density is shown. According to the manufacturers (Cospheric for all particles except ones made of tungsten which come from US Research Nanomaterials Inc), few particles are smaller than the indicated size range and not more than 10% of microparticles are larger than the indicated size range. This accords with the distribution of sizes measured in subsequent data. The particles were placed in 96% v/v ethanol at a concentration of 3% w/w and vortexed immediately prior to pipetting 20 μL onto macrocarriers. Note that the experiments are analysed one particle at a time to relate penetration depth to

particle size, so the results are not affected by possible differences between the particle size distribution on the macrocarriers (suspension taken from the bottom of the test tube might be enriched in faster-settling larger particles). Ethanol was allowed to evaporate three hours in a desiccator at ambient temperature and pressure before particles were used. Microparticle penetration was characterized in three gels and three cornea samples for all materials tested.

Table 1 – Information About Particles Used

Particle Material	**Particle Density**	**Size (Diameter) Range**
poly(ethylene)	1.1 g/cc	10 – 29 μm
soda-lime glass	2.5 g/cc	10 – 22 μm
barium-titanate glass	4.2 g/cc	5 – 22 μm
stainless steel	7.8 g/cc	5 – 22 μm
tungsten	19.2 g/cc	20 – 40 μm

2.3. Tissue Processing for Penetration Depth Measurements

Following particle delivery, porcine eyes were placed in Falcon vortex tubes filled with Davidson's Fixative Solution (DFS, as described in Shariati et al., 2008). Whole eyes were allowed to be fixed for two hours so the cornea would maintain its natural shape, and then corneal tissue was dissected from intact globes, placed in DFS, and refrigerated for 24 hours. Tissue was transferred from DFS to 10% w/w sucrose in PBS for eight hours followed by 30% w/w sucrose in PBS overnight. Fixed cornea tissue was trimmed to a 1 cm square and frozen in optimal cutting temperature (OCT) compound for 1 hour at -80 °C. Sections were prepared on a microtome in a cryostat to a thickness of 50 μm (larger than the largest particle size) and were imaged immediately to collect data on particle positioning within the tissue. Gel samples were sufficiently stable to section manually using a razor blade in order to photograph particle-field cross-sections. To collect statistics on particle penetration into gelatin or corneal tissue, an image processing pipeline was developed in which individual particles are selected, particle diameter is measured, and the distance from the surface of the specimen is calculated (pipeline shown in Supplementary Information S1).

2.4. Therapeutic Microparticle Preparation

To assess the ability of delivering bulk therapeutic compounds to the cornea's anterior surface, poly(ethylene glycol) (PEG) microspheres with 1% w/w Eosin Y were prepared using a spray-drying technique. A vibrating orifice aerosol generator (Berglund et al., 1973) with a 35 μm pinhole ejecting droplets at 5 m/s with a piezoelectric ceramic vibrating at 30 kHz was used to produce droplets of 3.96% w/w PEG with 0.04% w/w Eosin Y in 96% v/v ethanol. Droplets fell through a 1-meter-tall 10-cm-diameter drying column equipped with ports for heated, dry gas. N_2 at 100 °C with a flowrate of 30 standard cubic feet per hour was used to heat and carry the smaller particles through the column. Large (100 μm) droplets had a settling time in the column of around 5 seconds. Microparticles were collected at the bottom of the drying column and further dried in a vacuum oven overnight (at ambient temperature) before being placed on macrocarriers.

2.5 Assessment of Tissue Damage Using Confocal Microscopy

Confocal microscopy was done on tissue treated with stainless steel microparticles prior to staining with picosirius red (from Abcam Inc.). Picosirius red is a fluorescent dye that binds strongly to collagen fibrils and also stains epithelial tissue. Sections of tissue were cut to 30 μm thickness and were then stained for 5 minutes. This was sufficient to produce bright fluorescence on the stroma and the epithelium. Tissue was inspected using a Zeiss LSM 710 inverted confocal microscope. Z-stacks were recorded (30 μm depth) to show how the tissue is damaged as a result of microparticle impact.

3. Results

3.1. Penetration of Microspheres in 5% w/w Ballistic

To validate the particle delivery method, imaging and image processing pipeline, ballistic gelatin was used as a well-established reference material. Representative micrographs of particles embedded in 5 % w/w gelatin are shown in Fig. 1. The image processing pipeline used processes individual frames, isolates objects with an intensity below a certain threshold, and generates the statistics reported. Each scatterplot shows the result of 300 impacts into the homogeneous material. Statistics were generated based on data from impacts in 5 % w/w gelatin, and data in Supplementary Information qualitatively describes penetration in 2.5 % w/w and 10.0 % w/w ballistic gelatin. The image processing pipeline measured microparticles that are within the expected size distribution. Some microparticles are larger than the expected range, which is expected since the vendor reports 10% of particles have sizes larger than the reported range.

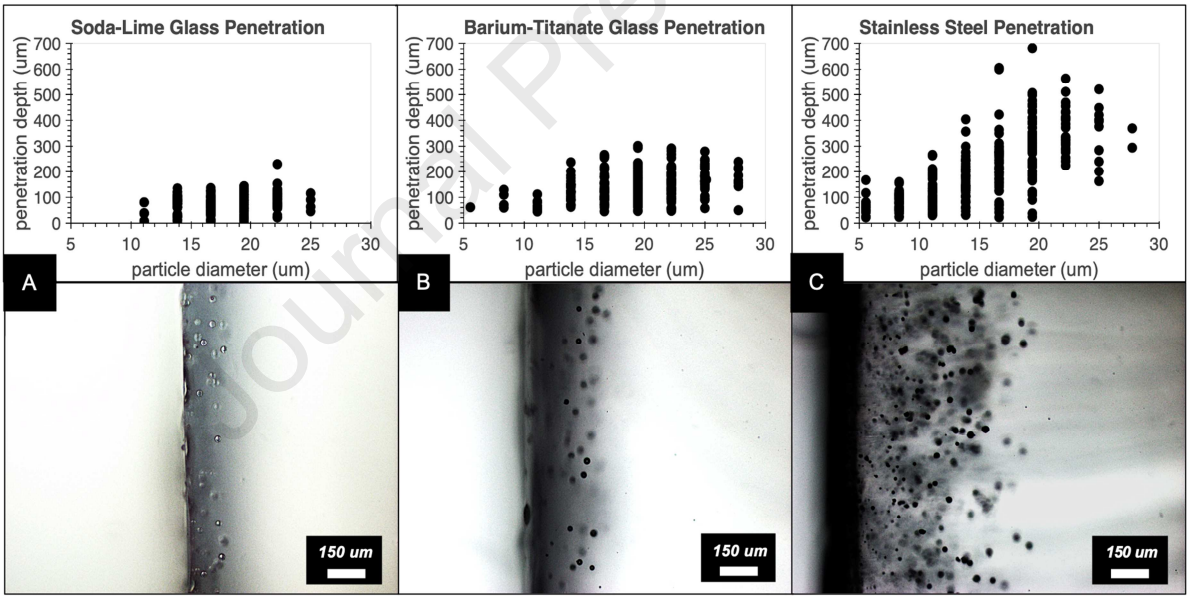

Fig. 1 – demonstration of particle embedding energies in 5 % w/w gelatin. Penetration depth of particles from three shots to gelatin and representative images for A) soda-lime glass particles, B) barium-titanate particles, and C) stainless-steel particles.

To show the consistency of the ballistic device, mean penetration depths are reported for three different size groupings for soda-lime glass, barium-titanate glass, and stainless steel microparticles. The results of this analysis are shown in Fig. 2.

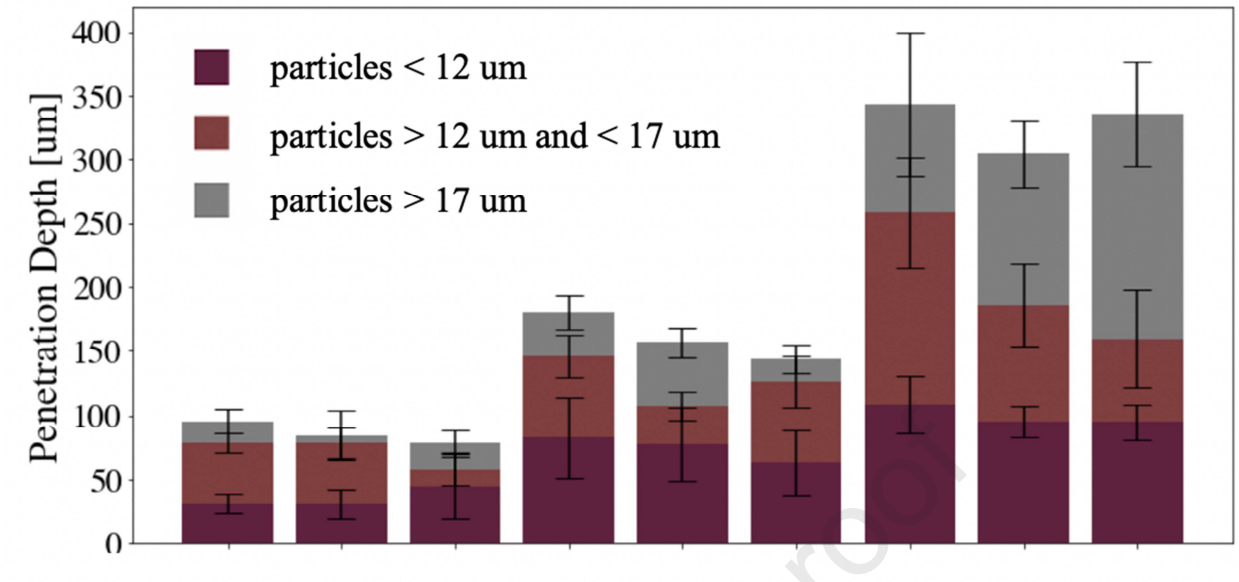

Fig. 2 – average penetration depth for each of three replicate doses of polydisperse particles delivered into gelatin. The overall bar is the average over relatively large particle diameters; the intermediate bar is the average over particles of intermediate diameter, and the lowest bar is the average over relatively small particles. Error bars show 95% confidence intervals of the penetration depth distribution. SL1 = soda-lime glass shot #1, BT2 = barium-titanate glass shot #2, and SS3 = stainless steel shot #3.

3.2. Penetration of Model Microspheres in Cornea Tissue

By processing image data from sections of corneal tissue exposed to ballistic microparticles, the statistics shown in Fig. 3 were recorded. Each scatter plot shows the result of 300 particles identified in tissue. The particles were identified and their dimensions indicated by a user of the image processing pipeline. This was done instead of thresholding image intensity data, because there were defects in the image data that came from reflections off of the tissue which made it difficult to identify objects from thresholding alone. There are slight variations in the thickness of the epithelium. The thickness of the epithelium was measured for 100 images of corneal sections. The average thickness was 63.1 μm (standard deviation of 9.8 μm). Despite areas where the epithelium was thinner, there is little ability for the microparticles tested to carry through the epithelium and embed into the stromal tissue of the cornea.

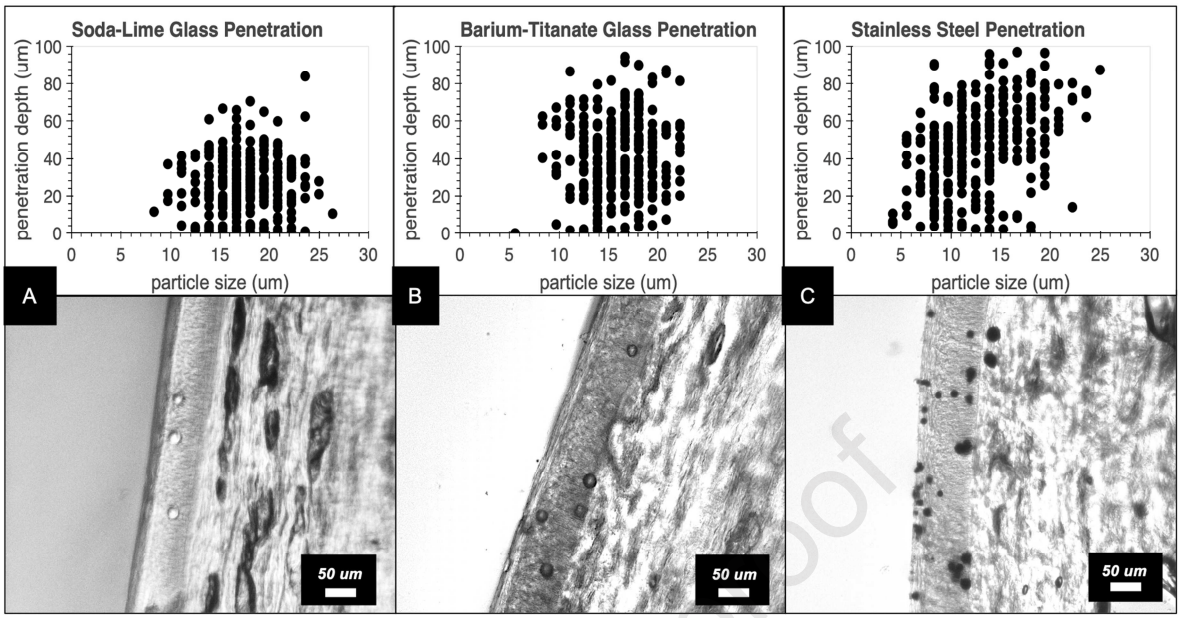

Fig. 3 – particle embedding in corneal tissue. Penetration depth of 300 particles from three shots to porcine cornea and representative micrographs for A) soda-lime glass particles, B) barium-titanate glass particles, and C) stainless steel particles.

While all three particle compositions penetrate to a similar extent, there is more information contained in the probability density of particle impacts (Fig. 4 and Fig. 5). To calculate probability density, impact statistics are binned according to their distance from the sample surface. Then, binned penetration depths are divided by the total number of observations for that particle size. Penetration depth is normalized by dividing the penetration distance by particle diameter, so the expected proportionality to particle diameter yields a constant normalized penetration depth. In these figures, the "hotter colors" (purple and pink) represent areas where the probability density was greatest. In Fig. 5, the green bands represent the expected location of the interface between the epithelium and the stroma. When the average thickness of the epithelium is divided by the diameter of an expected particle, the green curve is generated. The dotted lines indicate upper and lower bounds of the epithelium interface calculated by using the standard deviation statistics recorded measuring the thickness of the epithelium.

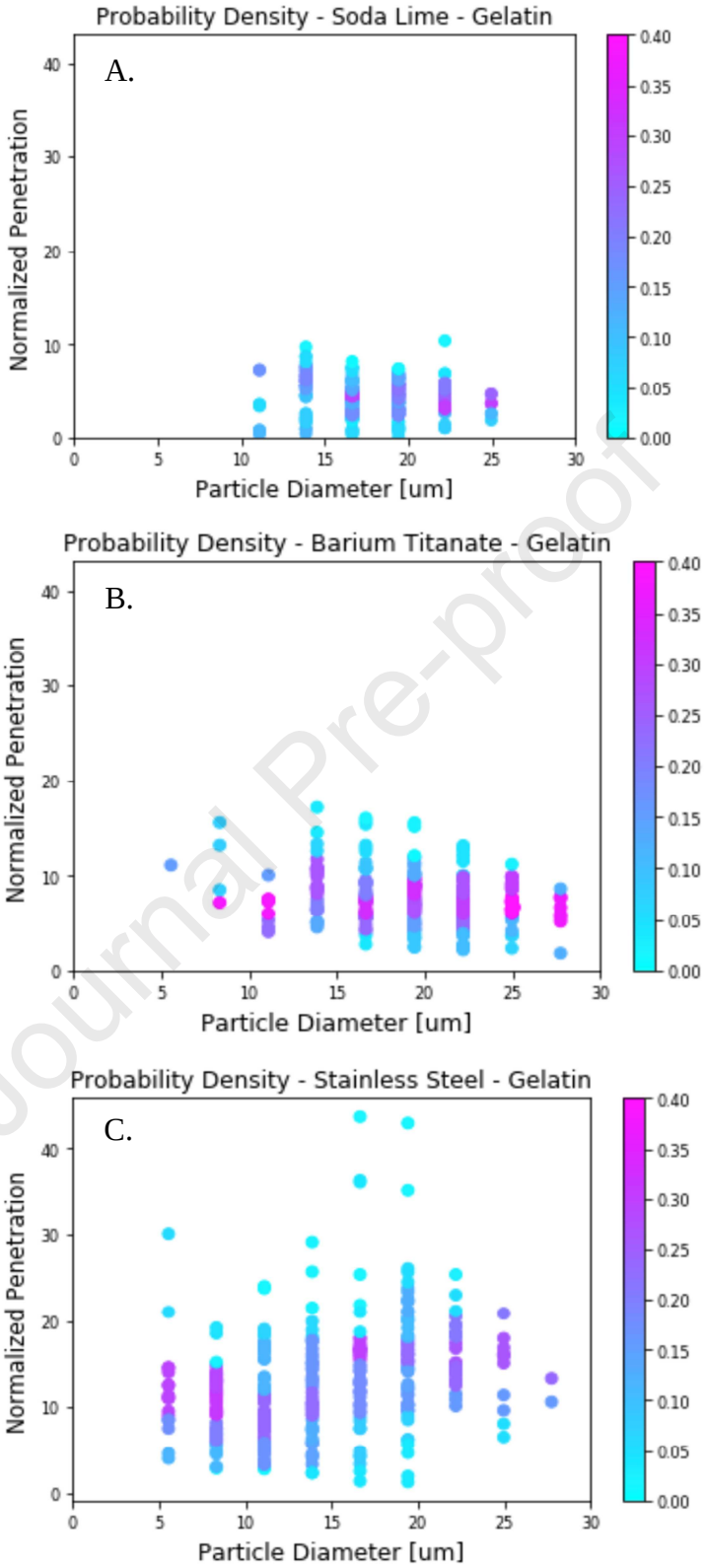

Fig. 4 – probability densities of soda lime, barium titanate, and stainless steel impacts in 5 % w/w ballistic gelatin shown with particle penetration normalized by particle diameter. Probability density for the colormap was calculated by binning data into discreet groups along the x and y axes.

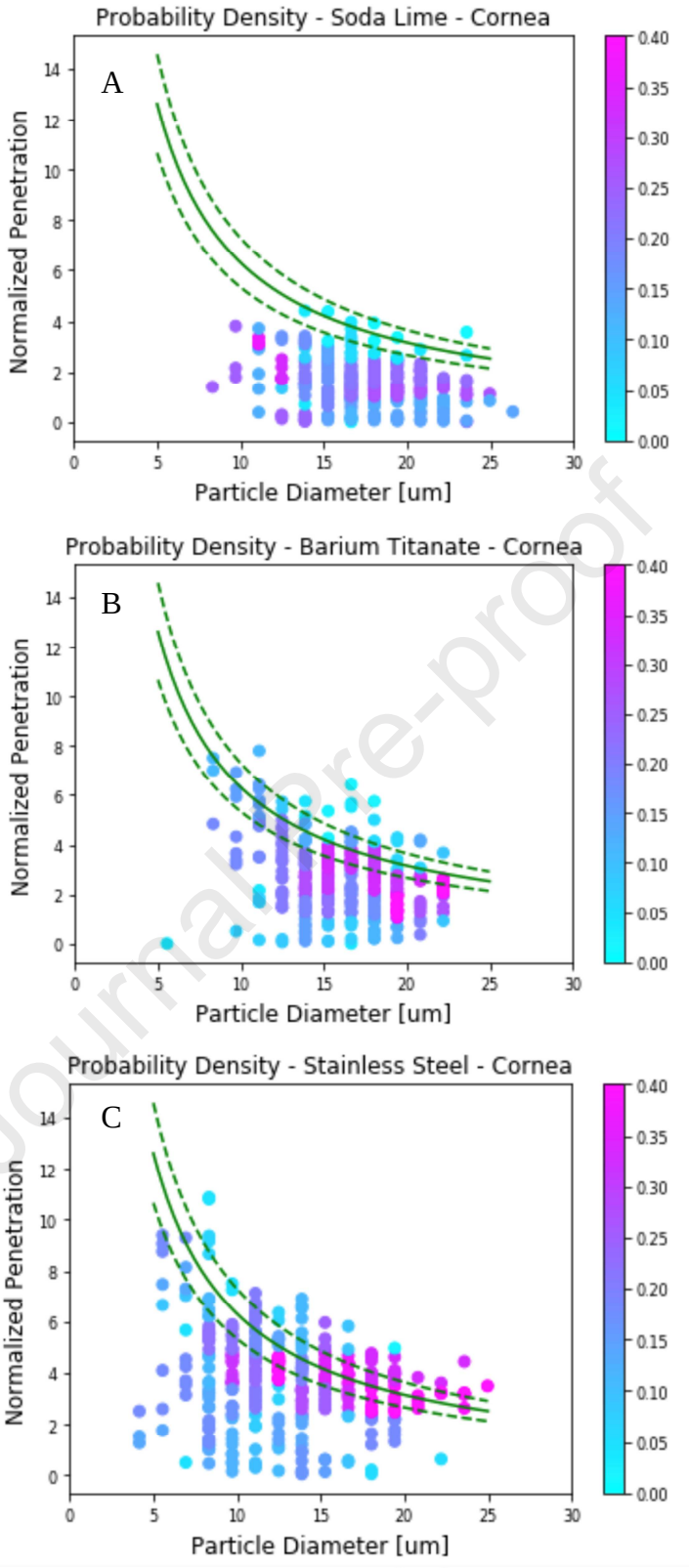

Fig. 5 – probability densities of soda lime, barium titanate, and stainless steel impacts in corneal tissue shown with particle penetration normalized by particle diameter. The green band represents the measured average thickness of the epithelial layer bounded by a standard deviation above and below the mean value.

To assess the ability for tissue to seal up as ballistic particles embed in the material, picosirius red was used to stain the epithelium and stroma and confocal microscopy was used to image individual layers of the tissue surrounding a single particle. A transmission micrograph indicating a single particle is shown in Fig. 6A. Images in Fig. 6B and 6C show individual frames from a z-stack measured around the same stainless steel particle in 6A.

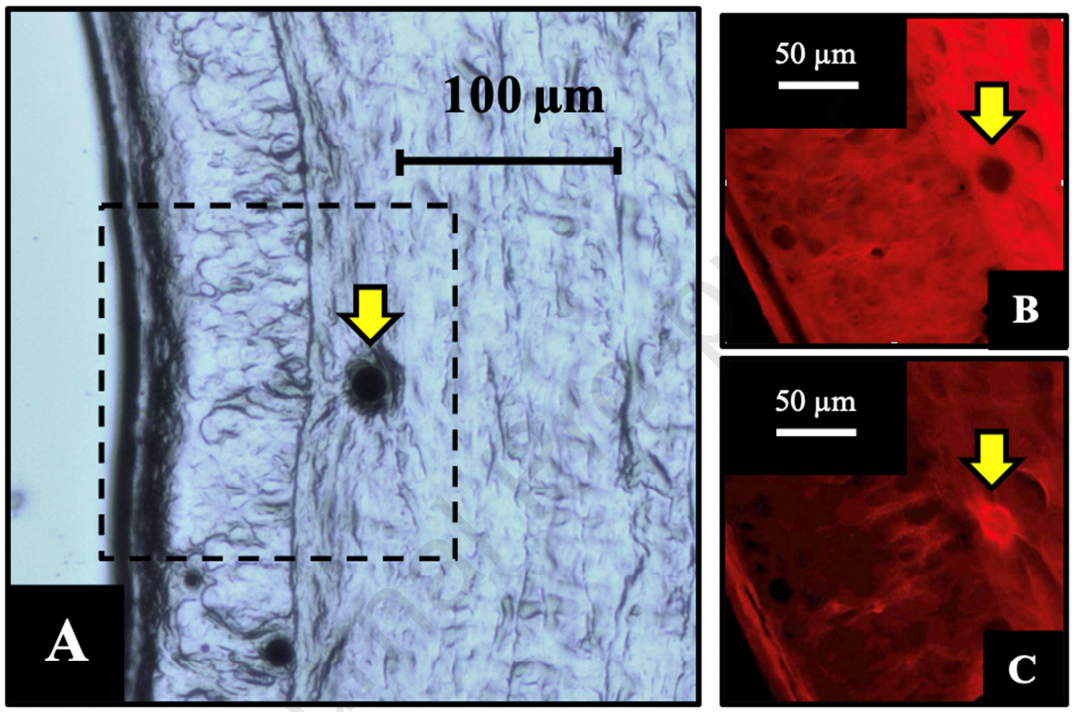

Fig. 6 – particles create low damage as the embed in tissue. A) Transmission micrograph of a stainless steel microparticle embedded in the stroma. Yellow arrow indicates a single 20 µm particle. B) Confocal micrograph of picosirius red stained, 30-µm-thick tissue section. Yellow arrow indicates same particle as in A). Image is 20 µm deep in the z-stack. C) Confocal micrograph from 10 µm deep in the z-stack.

3.3. Penetration of Low-Density Microparticles and Medicinal Microparticles

Lowest-density microspheres (1.1 g/cc poly(ethylene)) failed to demonstrate any significant embedding depth in gelatin or in corneal tissue. In Fig. 7A and 7B, it can be seen that these projectiles only embed in 5% w/w gelatin by one to three diameters. The embedding depth is much shallower than all other materials tested. Not surprisingly, when corneal tissue was tested with these particle payloads, penetration was superficial. Fig. 7C and 7D show fluorescent microparticles embedded just at the surface of tissue. Fig. 8A and 8B show PEG microparticles with 1% w/w Eosin Y embedded in the anterior surface of the cornea. These images were taken 10 minutes after ballistic delivery, and it can be seen that microparticles are dissolving into the surrounding tissue. Following the tissue fixation protocol two days later, Fig. 8C and 8D show the staining of the epithelium with Eosin Y. Microparticles have fully dissolved, and there is a strong staining of the corneal epithelium with the fluorescent Eosin dye. There is also considerable staining of the stroma below.

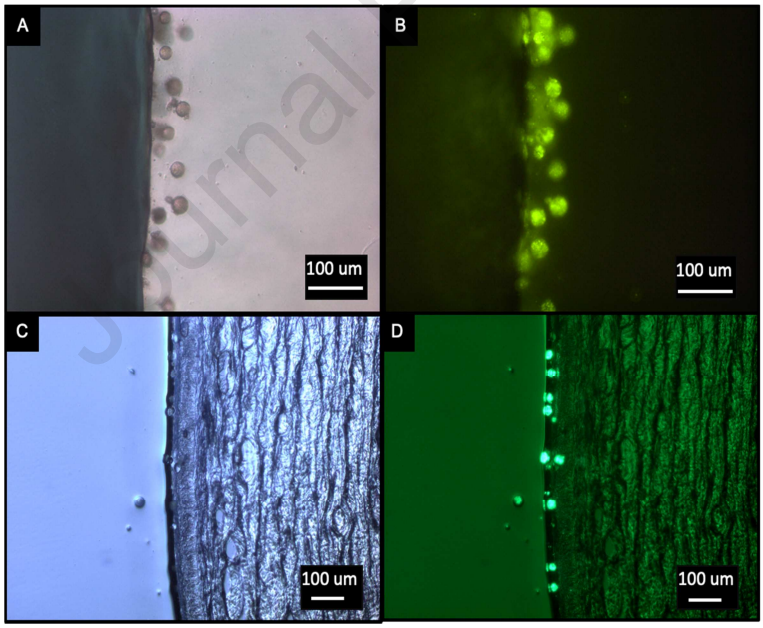

Fig. 7 – penetration of 1.1 g/cc polyethylene spheres in gelatin and corneal tissue. A) Bright-field microscopy of 5 % w/w gelatin. B) Fluorescent micrograph of gelatin. C) PE spheres in corneal tissue (brightfield). D) PE spheres in corneal tissue.

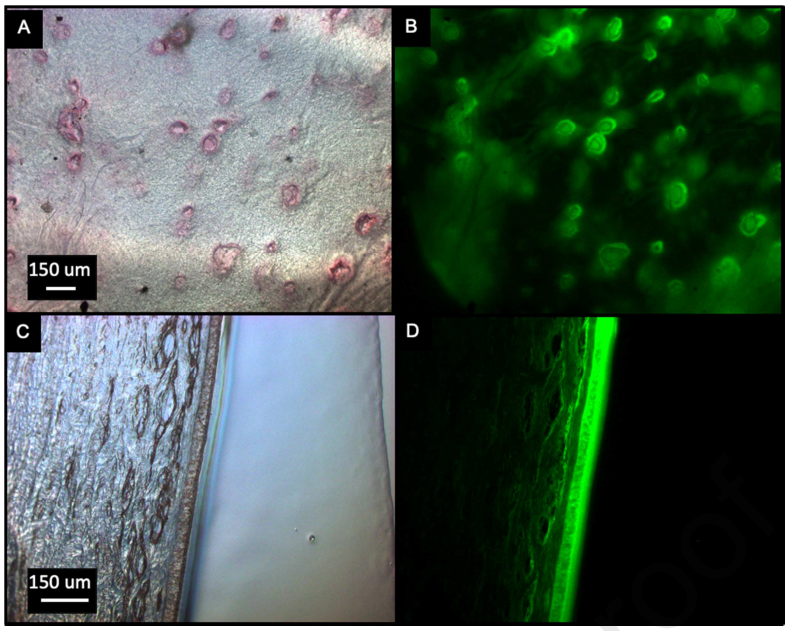

Fig. 8 – polyethylene glycol microspheres with 1% w/w EY embedded in corneal tissue. A) brightfield microscopy showing the anterior surface of the cornea ten minutes after treatment. B) Fluorescent excitation of anterior surface under 500 nm light excitation. C) 50 um thick cross section of corneal tissue two days later under brightfield and D) fluorescent microscopy

3.4. Penetration of Tungsten Particles and Debrided Corneal Tissue

A density was established at which microparticles infiltrate the stroma when tungsten was used as a projectile material. Fig. 9A shows the results of bombarding intact corneal tissue with tungsten particles. As can be seen, the tungsten microparticles just enter the superficial layers of stromal tissue. Despite having a density twice that of stainless-steel particles tested, there is only a small increase in the total penetration depth of microparticles. Fig. 9B shows the results of bombarding corneal tissue that has been debrided (epithelium removed with a razor blade). As can be seen, the stroma is an effective momentum sink that arrests particles on its surface.

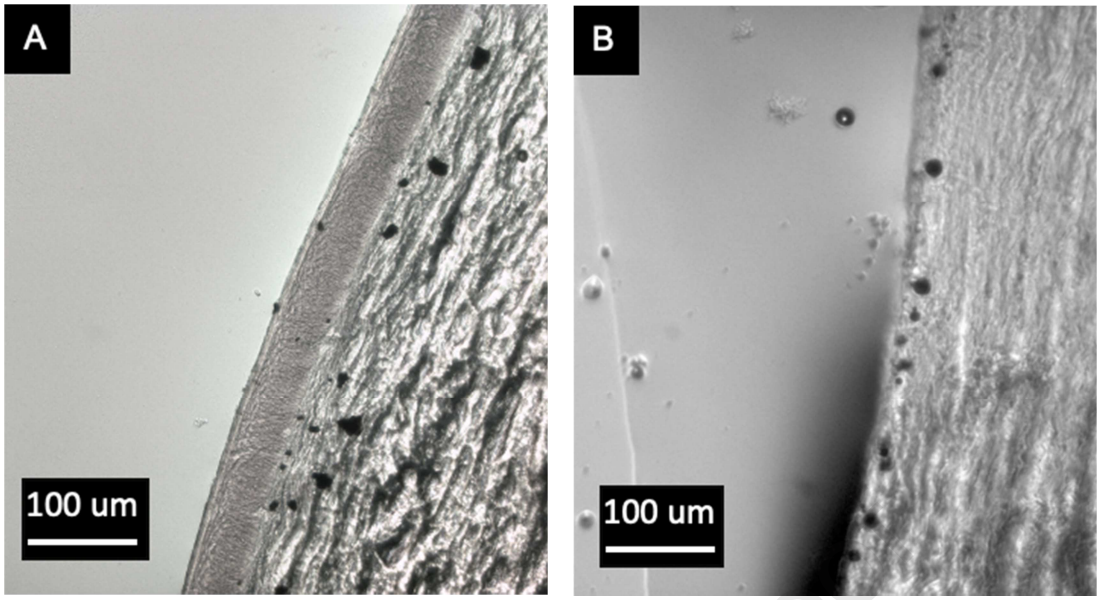

Fig. 9 – A) tungsten microparticles embedded to shallow depth in stroma. B) stainless steel microparticles in tissue with epithelium debrided prior to bombardment.

4. Discussion

In gelatin, penetration depth appears proportional to particle size and density, as is expected. Three concentrations of ballistic gelatin were examined (2.5, 5 and 10% w/w) for comparison with prior literature (Fig. 1 for 5% w/w ballistic gelatin; Supplementary Information S3 for other concentrations). The mean and standard deviation of penetration computed for each of three replicate experiments shows good reproducibility (Fig. 2): with the exception of the middle-size range for stainless steel, the mean penetration depth for each of three particle diameter groupings are indistinguishable (no statistically significant difference from experiment-to-experiment). This indicates that particle penetration data is comparable each time the ballistic device is actuated. Using the results of Veysset *et al*., who show penetration of microparticles into ballistic gelatin conforms to the Poncelet Model (loss of kinetic energy predominantly due to work of fracture) and provide resistance values for the three concentrations examined in this work, we can infer the distribution of impact velocities (Supplementary Information, S4). The results indicate the velocity of most microparticles is in the range 150 to 300 m/s, with some particles having impact velocity inferred to be as high as 500 m/s.

Penetration depth z_∞ in uniform, isotropic gelatin and viscoelastic fluids is known to scale with the Elastic Froude Number $\frac{z_\infty}{2r_p} \sim \left[\frac{\Delta\rho v^2}{E}\right]^\gamma$, where $\Delta\rho$ indicates density difference relative to the target material, v is the impact velocity, E is the shear storage modulus of the substrate, r_p is the particle radius, and γ is an exponent empirically found to be between 1/3 and 1/2 for projectiles orders of magnitude larger than what is used here (Akers et al., 2006; Swain et al., 2014). In Swain et al., this dimensionless group included a difference between the impact velocity and a threshold velocity for embedment, which was proportional to the contact pressure. The estimated impact velocity was used alone in this analysis, due to insufficient knowledge of particle velocity. Direct measurement of particle velocity was not performed, due to the ballistic embedment process being enclosed in a sealed vacuum chamber that made it difficult to film embedment with high-speed imaging. Penetration in this dataset is observed to scale with the Elastic Froude Number to a power of 0.8 ± 0.2 (calculated in Supplementary Information S2).

The results in gelatin lay the foundation for interpreting the particle penetration observed in the cornea, which is dramatically different. Both small and large particles embed to similar depths in the corneal epithelium. Like the images shown in Fig. 3, most particles can be found between 30 and 60 μm deep. The probability density for the normalized penetration depth in ballistic gelatin is insensitive to particle size, as expected (Fig. 4). In gelatin, increasing relative density of the particles relative to the sample conforms with the expected proportional increase in normalized penetration. In contrast, normalized penetration into the cornea is not independent of particle size and does not simply increase proportionally with the particles' relative density (Fig. 5).

Peculiar features of the distribution of normalized penetration in the cornea include possible evidence of bimodal probability distributions for small, low density particles (Fig. 5A, 12.5±0.7 and 14.0±0.7; for smaller particles, very few entered the epithelium and loss of particles from the surface during handling precluded quantitation). A first peak at very low penetration suggests that there is a threshold impact velocity required to pass through the apical layer of the corneal epithelium (*i.e.*, the distribution of impact parameter for small soda lime particles includes some that are so low that the particles come to rest on the epithelium). With increasing size, soda lime particles transition to a unimodal distribution as seen in ballistic gelatin, with the most

probable normalized penetration that is insensitive to particle size (Fig. 5A, for particle diameter > 15 μm). At the opposite extreme, large, high density particles show a penetration depth that does not increase with particle size and normalized penetration depth actually decreases with increasing particle size (Fig. 5B for particle diameter > 15 μm and Fig. 5C for particle diameter > 8 μm). The peak penetration depth appears to be dictated by the thickness of the epithelium (indicated by a shaded band in Fig. 5). The limited ability of the microparticles tested to penetrate through the epithelium and embed into the stromal tissue of the cornea suggests that there is a threshold remaining kinetic energy that must be exceeded for particles to pass through the boundary between the epithelium-stroma. In accord with this hypothesis, the distribution of penetration depths has a pronounced asymmetry, with an abrupt decrease in probability of penetration into the stroma.

When particles enter the cornea, it appears that there is a narrow range of penetration depths in which particles can embed, confined to the epithelium for the range of impact parameter examined here. Once particles reach the epithelial-stromal boundary, their motion is essentially arrested. This behaviour accords with corneal mechanical properties in the literature. Atomic force microscopy (AFM) has been applied to interrogate individual layers, leading to a Young's Modulus of 0.57 kPa for the corneal epithelium, 110 kPa for Bowman's Layer, and 33 kPa for the stroma (Last et al.; 2012). While porcine corneas lack Bowman's Layer, mechanical properties within the stroma can be stiff and vary with depth. Regions where the collagen lamellae are more interwoven (the anterior stroma) are consistently found to be stiffer than the posterior cornea (Blackburn et al., 2019). Such a step up in the stiffness could explain the high probability of particles halting at the boundary between the two layers. We considered the possible role of the epithelial basement membrane and concluded that for the porcine corneas considered here it is unlikely to make a significant contribution to arresting particle penetration: it is quite thin (~100 nm thick) and is continuous with the stroma below (Abhari et al., 2018). Nonetheless, the evidence reported in this research suggests layered heterogeneity in mechanical properties of tissue is what gives rise to the cornea's penetration response.

While embedding was shallow, it is interesting to note that penetration into the epithelium did not leave a visible "track." To the extent observable with optical microscopy, no evidence of tissue damage was seen. When tissue was examined using

confocal microscopy, there also was no evidence of noticeable tracks left in tissue. The results show the particle firmly embedded in collagen fibrils in Fig. 6C. There is a local compression of the fibers surrounding the particles and a bright fluorescent signal. The integrity of the epithelium can be seen clearly in Fig. 6B. This frame shows that there are no clear tracks left by the particle in the epithelial layer. This suggests that the ballistic treatment is non-destructive – as particles travel through tissue in the embedding process, the material has the ability to reseal behind the particle. This elastic response is akin to the formation and subsequent collapse of smooth cavities that form when ballistics penetrate homogeneous materials, like ballistic gelatin. This result is promising and indicates that while there may be local compression of tissue, there are no visible channels left behind penetrating particles.

By using tungsten microparticles (density is 19.2 g/cc), there was effective embedment of microparticles in the corneal stroma. To the best our knowledge, this is the first example of ballistic microparticles traversing the epithelium and accessing underlying stromal tissue. However, this result highlights how effective of a momentum sink the corneal stroma is - only with exceptional high density can embedment in the tough fibers of the stroma be achieved. Even with the epithelium completely removed, stainless-steel microparticles still only embed in the stroma to a superficial distance. The stroma does appear to be an effective stopping medium for ballistic microparticles. While the corneal epithelium appears to be able to slow particles down slightly (especially smaller particles), it is likely, considering these experiments, that the primary barrier to microparticle uptake is the stromal interface.

Penetration of lowest density microparticles (polyethylene; 1.1 g/cc) was shallow in gelatin and was superficial in corneal tissue. Clearly, when target and particle density are equivalent, significant penetration is prevented. A similar result was observed when custom, therapeutic microparticles are delivered to corneal tissue. Despite low penetration depth of projectiles, there was still efficient distribution of therapeutic compound to the cornea. While the epithelium shows most of the staining, there was some staining of the underlying stroma as well. Perhaps having small particles that embed in the apical surface of the cornea that slowly dissolve is a preferable mode of drug-delivery compared to topical administration of drug solution.

While this study did not uncover facile uptake of microparticles in the stroma, useful information was uncovered about just how well the cornea is protected from high velocity microparticles. This material responds as well, if not better, than skin tissue as a stopping medium (Kendall et. al, 2000; Kendall et. al, 2004). Toughness demonstrated by this tissue is even more surprising, considering the cornea has a higher water constant than skin tissue. The cornea has a reported water content of 76% by mass (Hedbys et al.,1966), much higher than the exposed surface of the skin's stratum corneum, which contains 40% water at the surface and increases to 70% water by the stratum granulosum (Warner et al. 1988).

5. Conclusions

Using gelatin as a reference material provides a means to confirm that the velocity distribution of particles provided by a PDS1000 "gene gun" is insensitive to particle density and particle diameter even in the range of 5-25 μm diameter and particle density up to 7.8 g/cm^3. Literature values for the properties of ballistic gelatin enable estimation of the distribution of particle velocities (150-500m/s). This information makes particles with a distribution of diameter and velocity valuable for interrogating the mechanical properties of a biological tissue. The dramatic difference in penetration distribution seen in corneal tissue compared to gelatin provides clear evidence of enhanced barrier function at the anterior surface of the corneal epithelium and especially at the interface between the epithelium and the stroma. Using a ladder of particle densities expanded the range of impact kinetic energy to span from values low enough that a significant fraction of particles halt at the anterior surface up to values that result in a majority of particles penetrating entirely through the epithelium and coming to a halt at or near the interface between the cornea and the stroma. The stroma is an effective stopping medium, worthy of further investigation with methods that provide higher particle velocity. Laser Induced Projectile Testing can reach velocities of 3,000 m/s with silica particles (Veysset et al, 2020). In addition to higher particle velocities, examination of long-slender particle shapes that give sectional density comparable to steel spheres may enable penetration into the stroma.(Zhang et al., 2017).

There may be utility to using ballistic therapeutic microparticles for drug delivery to the cornea. Bioavailability of therapeutic compounds in topically delivered eye drops is low (as little as 5%), with most of the topically administered formulation

washed away within just 15–30 s after instillation (Ahmed, 2003). The present study suggests an alternative: drug laden microparticles could be uniformly delivered to the epithelium. In addition to revealing surprising penetration mechanics, understanding the biolistic delivery of microparticles may deserve investigation as a solution to the problem of low bioavailability of drugs delivered topically to the eye.

Acknowledgements: We would like to acknowledge Professor Alex Groisman for getting our group started with technology for ballistics research. Also, we would like to thank Professor Guruswamy Ravichandran for fruitful discussions regarding impact mechanics.

Funding: We would like to thank Sakura Finetek for funding to complete this research. Also, we would like to thank The Jacobs Institute for Molecular Medicine for funding and the Rosen Center for Bioengineering. We would also like to thank the Caltech Biotechnology Leadership Program (a pre-doctoral program focusing on Micro/Nano medicine) for their support through NIH grant T32GM112592.

Data Availability Statement: The data that support the findings of this study are available from the corresponding author upon request.

Bibliography

1. Abhari, S. Eisenback, M., Kaplan, H., Walters, E., Prather, R., & Scott, P. Anatomic Studies of the Miniature Swine Cornea. *Anat. Rec.* 301, 1955–1967 (2018).
2. Ableson, M., Maffei, C. & Howe, A. Why Doesn't the Ocular Drug Work? A look at the various barriers and aids to the efficacy of ocular medications. *Rev. Opthalmology* (2009).
3. Ahmed, I. The noncorneal route in ocular drug delivery. in *Ophthalmic drug delivery systems* 335–63 (2003).
4. Akers, B. & Belmonte, A. Impact Dynamics of a Solid Sphere Falling into a Viscoelastic Micellar Fluid. *J. Nonnewton. Fluid Mech.* **135**, 97–108 (2006).
5. Berglund, R. N. & Liu, B. Y. H. Generation of Monodisperse Aerosol Standards. *Environ. Sci. Technol.* **7**, 147–153 (1973).
6. Bidwell, G., Liu, H., Robinson, J., Marquart, M. & George, E. A corneal penetrating drug delivery system based on elastin-like polypeptide. *Fed. Am. Soc. Exp. Biol.* **28**, 1 (2014).
7. Blackburn, B. J., Jenkins, M. W., Rollins, A. M. & Dupps, W. J. A review of structural and biomechanical changes in the cornea in aging, disease, and photochemical crosslinking. *Front. Bioeng. Biotechnol.* **7**, (2019).
8. Camodeca, A. & Anderson, E. Corneal Foreign Body. *StatPearls.* 1-10 (2020).
9. Cifariello, F., Minicucci, M., Di Renzo, F., Di Taranto, D., Coclite, G., Zaccaria, S., De Turris, S., & Costagliola, C. Epi-Off versus Epi-On Corneal Collagen Cross-Linking in Keratoconus Patients: A Comparative Study through 2-Year Follow-Up. *J. Ophthalmol.* (2018).
10. Daull, P., Amrane, M. & Garrigue, J.-S. Novasorb® Cationic Nanoemulsion and Latanoprost: the Ideal Combination for Glaucoma Management? Journal of Eye Diseases and Disorders. *J Eye Dis Disord* **2**, 1 (2017).
11. Gordon-Shaag, A., Millodot, M., Shneor, E. & Liu, Y. The genetic and environmental factors for keratoconus. *Biomed Res. Int.* 2015, 24–32 (2015).
12. Gumus, K., Karakucuk, S. & Mirza, E. Corneal Injury From a Metallic Foreign Body: An Occupational Hazard. *Eye Contact Lens Sci. Clin. Pract.* 33, 259-260 (2007).

13. Hedbys BO, Mishima S. The thickness-hydration relationship of the cornea. *Experimental Eye Research*, 5(3):221-228 (1966).
14. Huynh, J. Factors Governing Photodynamic Cross-Linking of Ocular Coat. (2011).
15. Jia, H. Z. & Peng, X. J. Efficacy of iontophoresis-assisted epithelium-on corneal cross-linking for keratoconus. *Int. J. Ophthalmol*. 11, 687–694 (2018).
16. Jussila, J. Preparing ballistic gelatin - Review and proposal for a standard method. *Forensic Sci. Int.* 141, 91–98. 141, 91-98. (2004).
17. Kendall, M. A. F., Wrighton Smith, P. J. '92 & Bellhouse, B. J. Transdermal Ballistic Delivery of Micro-Particles: Investigation into Skin Penetration. *BS EMBS Int. Conf*. (2000).
18. Kendall, M., Mitchell, T. & Wrighton-Smith, P. Intradermal ballistic delivery of microparticles into excised human skin for pharmaceutical applications. *J. Biomech.* **37**, 1733–41 (2004).
19. Last, J. A., Thomasy, S. M., Croasdale, C. R., Russell, P. & Murphy, C. J. Compliance profile of the human cornea as measured by atomic force microscopy. *Micron.* 43, 1293–1298 (2012).
20. Lu, W. N. et al. Gene transfer into corneal endothelial cells by Helios gene gun. *Nihon. Ganka Gakkai Zasshi*. 107, 189–195 (2003).
21. Merediz, S. A. K., Zhang, E. P., Wittig, B. & Hoffmann, F. Ballistic transfer of minimalistic immunologically defined expression constructs for IL4 and CTLA4 into the corneal epithelium in mice after orthotopic corneal allograft transplantation. *Graefe's Arch. Clin. Exp. Ophthalmol*. 238, 701–707 (2000).
22. Mitchell, T., Kendall, M. & Bellhouse, B. A ballistic study of micro-particle penetration of the oral mucosa. *Int. J. Impact Eng*. 28, 581–99. (2003).
23. Scott, R. The injured eye. *Philos. Trans. R. Soc. B Biol. Sci*. 366, 251–260 (2011).
25. Shariati, A., Ameri, H. ., Hinton, D. . & Humayun, M. The Effects of Davidson's Fixative Solution in Preserving the Rabbit Eye. *Investig. Opthalmology Vis. Sci.* 49, (2008).
26. Swain, M., Kieser, D., Shah, S. & Kieser, *J. Projectile Penetration Into Ballistic Gelatin*. *J. Mech. Behav. Biomater.* **29**, 385–92 (2014).
27. Tanelian, D. L., Barry, M. A., Johnston, S. A., Le, T. & Smith, G. Controlled gene gun delivery and expression of DNA within the cornea. *Biotechniques* 23,

484–488 (1997).

28. Veysset, D. et al. High-velocity micro-particle impact on gelatin and synthetic hydrogel. *J. Mech. Behav. Biomed. Mater.* 86, 71–76 (2018).
29. Veysset, D., Sun, Y., Kooi, S. E., Lem, J. & Nelson, K. A. Laser-driven high-velocity microparticle launcher in atmosphere and under vacuum. *Int. J. Impact Eng.* **137**, (2020).
30. Warner, R.R., Myers, M.C., Taylor, D.A. Electron probe analysis of human skin: determination of the water concentration profile. *J Invest Dermatol*, **90**: 218–224 (1988).
31. Zhang, E. P. et al. Minimizing side effects of ballistic gene transfer into the murine corneal epithelium. *Graefe's Arch. Clin. Exp. Ophthalmol.* 240, 114–119 (2002).
32. Zhang, W. *et al.* Experimental investigation on ballistic stability of high-speed projectile in sand. *AIP Conf. Proc.* **1793**, (2017).

Declaration of interests

☒ The authors declare that they have no known competing financial interests or personal relationships that could have appeared to influence the work reported in this paper.

☒The authors declare the following financial interests/personal relationships which may be considered as potential competing interests:

There are no financial interests/personal relationships that may be considered potential competing interests.